Gating Charges in the Activation and Inactivation Processes of the hERG Channel

Mei Zhang, Jie Liu, and Gea-Ny Tseng

Department of Physiology, Virginia Commonwealth University, Richmond, VA 23298

ABSTRACT The hERG channel has a relatively slow activation process but an extremely fast and voltage-sensitive inactivation process. Direct measurement of hERG's gating current (Piper, D.R., A. Varghese, M.C. Sanguinetti, and M. Tristani-Firouzi. 2003. *PNAS.* 100:10534–10539) reveals two kinetic components of gating charge transfer that may originate from two channel domains. This study is designed to address three questions: (1) which of the six positive charges in hERG's major voltage sensor, S4, are responsible for gating charge transfer during activation, (2) whether a negative charge in the cytoplasmic half of S2 (D466) also contributes to gating charge transfer, and (3) whether S4 serves as the sole voltage sensor for hERG inactivation. We individually mutate S4's positive charges and D466 to cysteine, and examine (a) effects of mutations on the number of equivalent gating charges transferred during activation (z_a) and inactivation (z_i), and (b) sidedness and state dependence of accessibility of introduced cysteine side chains to a membrane-impermeable thiol-modifying reagent (MTSET). Neutralizing the outer three positive charges in S4 and D466 in S2 reduces z_a, and cysteine side chains introduced into these positions experience state-dependent changes in MTSET accessibility. On the other hand, neutralizing the inner three positive charges in S4 does not affect z_a. None of the charge mutations affect z_i. We propose that the scheme of gating charge transfer during hERG's activation process is similar to that described for the Shaker channel, although hERG has less gating charge in its S4 than in Shaker. Furthermore, channel domain other than S4 contributes to gating charge involved in hERG's inactivation process.

KEY WORDS: voltage-gated K^+ channel • ion channel gating • mutagenesis • Xenopus oocyte • voltage sensor

INTRODUCTION

Human ether-a-go-go related gene encodes the pore-forming subunits (hERG) of rapid delayed rectifier (I_{Kr}) channels expressed in the heart and several other cell types (Sanguinetti et al., 1995; Zhou et al., 1998; Emmi et al., 2000; Rosati et al., 2000; Shoeb et al., 2003). The hERG/I_{Kr} channel plays an important role in maintaining the electrical stability of the heart, as is suggested by the linkage between inherited or acquired long QT syndrome and mutations in the hERG gene or drug suppression of I_{Kr}. Relative to other voltage-gated K (Kv) channels, hERG manifests two unique gating properties. First, its activation process is relatively slow. At +50 mV, the time constant (τ) of activation is >50 ms for hERG, but <2 ms for the Shaker channel (Zagotta et al., 1994). Second, the inactivation and recovery from inactivation processes of hERG are extremely fast and voltage sensitive. Inactivation of hERG is due to conformational changes around the outer mouth region (Smith et al., 1996), similar to the "C-type" inactivation process first described for the Shaker channel (Hoshi et al., 1991). The τ of inactivation in the hERG channel ranges from 6.5 to 2.2 ms in the voltage range of −10 to +30 mV (corresponding to a gating charge of ∼0.7 e_o per channel), while τ of C-type inactivation in the Shaker channel in this voltage range is ∼2,000 ms and voltage insensitive (Hoshi et al., 1991). An important task in understanding the function of the hERG channel is to identify the structural basis for its unique gating properties.

hERG shares the basic structure design with other Kv channels (Fig. 1 A). It has four subunits arranged symmetrically around a central pore, with each subunit containing a voltage-sensing domain (S1–S4) and a pore domain (S5-P-loop-S6). Fig. 1 B aligns the amino acid sequences of transmembrane segments in the voltage-sensing domains of hERG, Shaker, bEAG (a close relative of hERG), and KvAP (a prokaryotic Kv channel whose crystal structure was solved) (Jiang et al., 2003a). Note that there is no consensus as to how the S4's positive charges in hERG or bEAG should be aligned with those in the Shaker (Schonherr et al., 2002; Smith and Yellen, 2002; Silverman et al., 2003), because a direct comparison of functional roles of these positive charges among the channels has not been available.

In terms of charge distribution in the voltage-sensing domain, hERG (as well as bEAG) differs from Shaker in

Address correspondence to Gea-Ny Tseng, Dept. of Physiology, Virginia Commonwealth University, 1101 E. Marshall St., Richmond, VA 23298. Fax: (804)828-7382. email: gtseng@hsc.vcu.edu

J. Liu's current address is Department of Pathophysiology, First Military Medical University, People's Republic of China.

Abbreviation used in this paper: WT, wild type.

J. Gen. Physiol. © The Rockefeller University Press • 0022-1295/2004/12/703/16 $8.00
Volume 124 December 2004 703–718
http://www.jgp.org/cgi/doi/10.1085/jgp.200409119

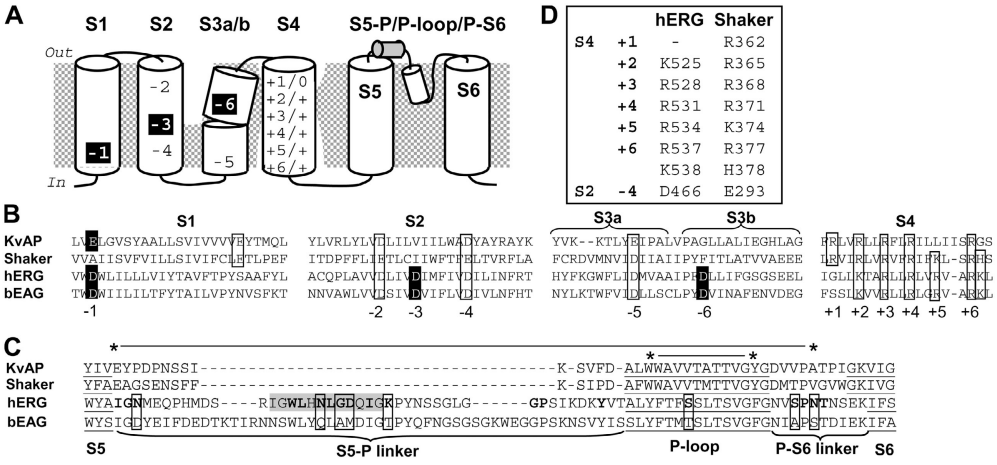

FIGURE 1. Basic structure design of voltage-gated K (Kv) channels and unique features in the hERG channel. (A) Two-dimensional transmembrane topology of a Kv channel pore-forming subunit, highlighting negative charges in S1, S2, S3a, and S3b (−2, −4, and −5 are conserved in all Kv channels, while −1, −3, and −6 are unique to EAG family members including hERG), and positive charges in S4 (+1 to +6 for Shaker/0 or + for EAG and hERG). The gray cylinder in the extracellular S5-P linker denote a putative α-helix formed by residues 583–594 in the hERG channel. (B) Alignment of amino acid sequences of S1, S2, S3a, S3b, and S4 of KvAP, Shaker, hERG, and b(ovine)EAG. Channel domains are denoted on top. Charged residues are boxed, and their generic numbers are marked below (−1 to −6, +1 to +6). (C) Alignment of amino acid sequences from the end of S5 to the beginning of S6 of KvAP, Shaker, hERG, and bEAG. Channel domains are denoted below. Asterisks connected by horizontal lines on top denote putative H bond donor/acceptor pairs around the outer mouth in Shaker and KvAP (Doyle et al., 1998; Larsson and Elinder, 2000), which are missing in the hERG and bEAG. Gray shade highlights hERG residues 583–594 that form a putative α-helix. The hERG residues that are critical for the channel's fast inactivation process are highlighted in bold (Liu et al., 2002). Boxes indicate bEAG residues that are different from hERG at these critical positions. (D) hERG residues examined in this study and the corresponding residues in the Shaker channel.

two aspects. First, the S4 domain in hERG has one less positive charge than that of Shaker. Second, in addition to the three negative charges in S2 and S3 that are well conserved in all Kv channels including Shaker (labeled as −2, −4, and −5; Fig. 1), hERG has three extra negative charges in its voltage-sensing domain (−1, −3, and −6; Fig. 1). The functional role of the positive charges in Shaker's S4 segment have been extensively studied (Aggarwal and MacKinnon, 1996; Seoh et al., 1996; Baker et al., 1998; Bezanilla, 2000; Cohen et al., 2003; Starace and Bezanilla, 2004; Horn, 2004). The generally accepted scheme is that the first four positive charges sense the transmembrane voltage and change their positions relative to the membrane barrier during channel activation (Aggarwal and MacKinnon, 1996; Seoh et al., 1996; Starace and Bezanilla, 2004). Therefore, these four residues are the "gating charges" in the Shaker channel. It is not known which of the positive charges in hERG's S4 segment carry gating charges during channel activation. Presumably the number of gating charges in hERG's S4 segment can influence its voltage sensitivity and thus the rate of activation (Logothetis et al., 1992, Islas and Sigworth, 1999, Starace and Bezanilla, 2004). The functional role of negative charges in the transmembrane segments of voltage-sensing domain has been well described for the Shaker and EAG channels (Tiwari-Woodruff et al., 2000; Papazian et al., 2002). These negative charges stabilize S4's positive charges by forming salt bridges. As S4 moves relative to the other transmembrane segments during gating, different charge pairings can occur that serve to stabilize the channel in the closed or open state (Tiwari-Woodruff et al., 2000; Papazian et al., 2002). Furthermore, in EAG channels, the extra negative charges in S2 and S3 can form a divalent cation (M^{2+}) binding site in the extracellular crevice around S4 (Silverman et al., 2000; Schonherr et al., 2002). It has been proposed that M^{2+}_o (Ca^{2+}_o or Mg^{2+}_o) binding here can restrict the crevice size and retard outward S4 movement during membrane depolarization, slowing down the channel's activation process (Silverman et al., 2000; Schonherr et al., 2002). Therefore, both positive and negative charges in the voltage-sensing domain contribute to determining the rate of channel activation.

Fig. 1 C aligns the amino acid sequences lining the outer mouth of hERG and other Kv channels. There are two unique features in hERG (and bEAG). First, hERG lacks some H bonds between residues around the outer mouth. Such H bonds have been proposed to exist in Shaker and other Kv channels (Doyle et al., 1998, Larsson and Elinder, 2000). Specifically, H bonds can be formed between the carboxylate side chain outside S5 (E418 in Shaker) and an amido nitrogen of the peptide backbone in the P-S6 linker (V450/G451 in Shaker) (Larsson and Elinder, 2000), and between nitrogens of two tryptophans and the hydroxyl group of a tyrosine at the two ends of the P-loop (W434/W435 and Y445 in Shaker) (asterisks connected by horizontal lines in Fig. 1 C) (Doyle et al., 1998). These H bonds serve to stabilize the outer mouth in the open state, slowing down the rate of C-type inactivation (Yang et al., 1997; Larsson and Elinder, 2000). In hERG, the corresponding residues

cannot form H bonds (Fig. 1 C). A reduced H-bonding capability in hERG can make its outer mouth more flexible than in the Shaker channel. Second, the S5-P linker is much longer in hERG (and bEAG) than in other Kv channels. Previously, we have shown that the central segment of the S5-P linker in the hERG channel (positions 583–597) plays a critical role in determining the degree of inactivation and K^+ selectivity (Liu et al., 2002). NMR spectroscopy showed that this segment may form an α-helix (termed "S5-P helix" in the following text) (Torres et al., 2003). We proposed that this S5-P helix can assume dynamic conformational changes during membrane depolarization, coming close to the pore entrance and participating in the outer mouth function (unpublished data). These features can contribute to the fast rate of inactivation in the hERG channel. However, one central question remains: what controls the voltage sensitivity of hERG's inactivation process? Arguments both for (Tristani-Firouzi, 2004) and against (Johnson et al., 1999) S4 as the voltage sensor for hERG's inactivation process have been made. In the latter case, no specific structural correlate has been proposed.

This study was designed to address the following questions: (1) which of the positive charges in hERG's S4 segment carry gating charges during channel activation, and (2) do they also serve the voltage sensor function for the inactivation process? In the Shaker channel, a negative charge at the cytoplasmic end of S2 (E293) may contribute to gating charge transfer (Seoh et al., 1996). Therefore, we also include the equivalent charge (D466) in our study. Fig. 1 D lists the hERG residues examined in this study and the corresponding residues in the Shaker channel. We apply two strategies in our experiments: (1) mutating charged residues and monitoring the effect on equivalent gating charges involved in activation and inactivation processes, and (2) testing the sidedness and state dependence of accessibility of cysteine side chains introduced into these charged-residue positions to a membrane-impermeable thiol-modifying reagent (MTSET). We discuss our results based on the "conventional gating model" (Ahern and Horn, 2004), instead of the recently proposed "paddle gating model" (Jiang et al., 2003b), because the latter model has been seriously challenged by experimental findings from Shaker and other Kv channels (Broomand et al., 2003; Cohen et al., 2003; Gandhi et al., 2003; Laine et al., 2003; Lee et al., 2003; Ahern and Horn, 2004; Horn, 2004; Starace and Bezanilla, 2004).

MATERIALS AND METHODS

Mutagenesis

hERG in a vector, pGH19 (a gift from G.A. Robertson, University of Wisconsin, Madison, WI), was subcloned into the Kpn I/Xba I site of pAlterMax. Mutagenesis was performed using the oligonucleotide-directed method and a commercial kit (Alter site II in vitro Mutagenesis System; Promega). Mutations were confirmed by direct DNA sequencing around the mutation sites. For transcription, plasmids were linearized by Not I and transcribed using T7 RNA polymerase using a commercial kit (mMessage mMachine; Ambion). The cRNA products were run on denaturing RNA gel along with RNA size markers, and their quality and quantity were evaluated using densitometry (ChemiImager model 4400; α-Innotech Corp). The mutant is designated by wild-type (WT) amino acid, followed by position number and the substituting amino acid using one-letter code.

Oocyte Preparation

Oocytes were isolated as described before (Tseng-Crank et al., 1990) and incubated in an ND96-based medium (composition given below), supplemented with 10% horse serum and penicillin/streptomycin at 16°C. 2–4 h after isolation, each oocyte was injected with 40 nl of cRNA solution (containing cRNA of 4–18 ng) using a Drummond digital microdispenser. Oocytes were incubated in the above medium at 16°C and studied 2–4 d after cRNA injection.

Voltage Clamp Experiments

Oocytes expressing cysteine-substituted mutants were pretreated with DTT (5 mM) before recording. Membrane currents were recorded from whole oocytes using the "2-cushion pipette" voltage clamp method (Schreibmayer et al., 1994). Both current-passing and voltage-recording pipettes had tip resistance 0.1–0.3 MΩ. During recordings, the oocyte was continuously superfused with a low-Cl ND96 solution to reduce interference from endogenous Cl channels. Voltage clamp was done at room temperature (24–26°C) with OC-725B or OC-725C amplifier (Warner Instruments). Voltage clamp protocol generation and data acquisition were controlled by pClamp5.5 via a 12-bit D/A and A/D converter (DMA; Axon Instruments). Current data were low-pass filtered at 1 kHz (Frequency Devices) and stored on disks for off-line analysis.

Data Analysis

The voltage clamp protocols and methods of data analysis are described in figure legends and text. The following software was used for data analysis: pClamp6 or 8, EXCEL (Microsoft), SigmaPlot, SigmaStat, and PeakFit (SPSS).

Cysteine Side Chain Modification

MTSET (Toronto Research Chemicals, Inc.) powder was dissolved in deionized water at 0.1 M shortly before experiments. The stock solution was stored on ice and used within 2 h. For extracellular application, after control data were obtained, the MTSET stock solution was diluted with bath solution to 1 mM and applied to the oocyte immediately. For intracellular application, a third fine-tipped pipette filled with MTSET stock solution was used to impale the oocyte. After confirming the stability of membrane currents, MTSET was injected into the oocyte. Assuming an oocyte volume of 0.5 μl (corresponding to a sphere of 1 mm diameter), injecting 10 nl of the stock solution would produce a cytoplasmic concentration of 2 mM immediately after the injection. The injection was controlled by the Drummond digital microdispenser as was used for cRNA injection.

Solutions

The ND96 solution had the following composition (in mM): NaCl 96, KCl 2, $CaCl_2$ 1.8, $MgCl_2$ 1, HEPES 5, Na-pyruvate 2.5, pH 7.5. The low-Cl ND96 used during voltage clamp experiments

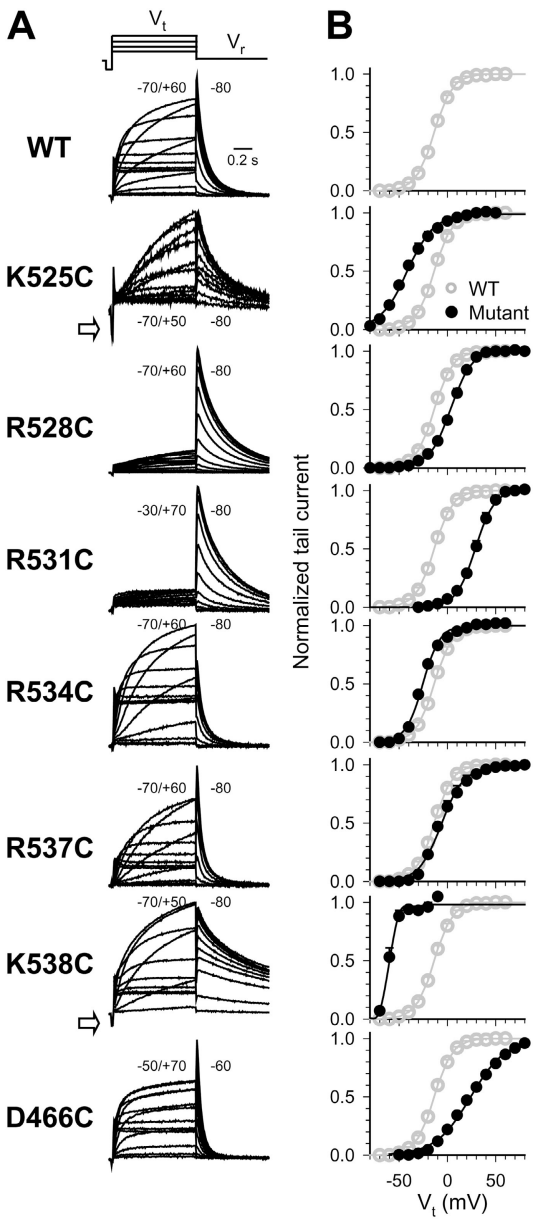

FIGURE 2. Effects of substituting S4's lysine (K) or arginine (R) with cysteine (C) on the channel function. (A) Original current traces from WT and mutants (specified on the left). The currents were elicited using the voltage clamp protocol diagrammed on top. From a negative holding voltage (V_h, −80 to −120 mV) 1-s test pulses to different test voltages (V_t) in 10-mV increments were applied once every 15 s. These were followed by repolarization to V_r. For each channel, the range of V_t (selected to cover the voltage range of channel activation) and the V_r level are marked adjacent to the current traces. The test pulses were preceded by a brief (10-ms) hyperpolarizing prepulse (−20 mV from V_h) whose purpose was to estimate the background channel conductance at V_h. Open arrows point to significant prepulse currents in K525C and K538C, reflecting channel opening at V_h. (B) Isochronal (1-s) activation curves of WT and mutant channels. For each cell, peak amplitudes of tail currents during V_r (I_{tail}, as shown in A) were normalized by the maximum tail current (I_{max}) obtained from the same cell after a strong V_t that maximally activated the channels. The relationship between normalized tail currents (I_{tail}/I_{max}) and V_t was fit with a simple Boltzmann function to estimate the half-maximum activation voltage ($V_{0.5}$) and slope factor (k): $I_{tail}/I_{max} = 1/[1 + \exp((V_{0.5} - V_t)/k)]$. To facilitate comparison, WT data are shown as gray symbols in all the panels for mutant channels (n = 6–14 each).

was made with Cl^- ions in ND96 replaced by methanesulfonate. In some experiments, [K] in low-Cl^- ND96 was raised to 20 mM. Equimolar [Na] was reduced to maintain the osmolality.

RESULTS

Effects of Charge Mutations on the Voltage Dependence of hERG Activation and Pore Domain Function

We first characterize the effects of charge mutations on the hERG channel function. The purpose is to evaluate how serious these single charge mutations can affect the structure–function relationship of the hERG channel. This information is important for the following experiments where we examine the effects of charge mutations on the channel's gating charges and use substituted cysteine side chains to deduce the accessibility of native side chains in the WT channel. Fig. 2 A shows test pulse currents of WT hERG and mutant channels during depolarization to various levels of V_t, and tail currents upon repolarization to V_r (V_t range and V_r marked adjacent to current traces). For each cell, the peak amplitudes of tail currents are normalized by the maximum tail current induced by a strong positive V_t to the plateau level of channel activation. This gives an estimate of the macroscopic channel open probability (P_o) at the end of the preceding test pulses. The relationship between V_t and P_o is used to construct the activation curves as shown in Fig. 2 B. For WT-hERG and all the mutant channels, the activation curves can be well described by a simple Boltzmann function:

$$\text{Normalized } I_{tail} = P_o = 1/[1 + \exp((V_{0.5} - V_t)/k)], \quad (1)$$

where $V_{0.5}$ and k are the half-maximum activation voltage and slope factor. The numerical values of $V_{0.5}$ and k for the WT and mutant channels are listed in Table I.

Neutralizing the positive charges at the two ends of S4, K525C, and K538C causes a prominent hyperpolarizing shift in the activation curve and induces channel opening at the negative holding voltage (Fig. 2 A, white arrows). R534C also causes a modest but statistically significant hyperpolarizing shift in the activation curve. Thus, these three mutations stabilize the open state, relative to the closed state, of the hERG channel. Neutralizing the other three positive charges in S4 (R528C, R531C, and R537C) and D466 in S2 causes differing degrees of depolarizing shift in the activation curve, indicating a stabilizing effect on the closed states relative to the open state of the hERG channel.

TABLE I

Effects of Cysteine Substitution of Charged Residues in S4 and S2 on hERG Channel Function

Channel	$V_{0.5}$[a]	k[a]	*n*	z_g[b]	$\Delta\Delta G_o$[c]
	mV	*mV*		e_o	*kcal/mol*
WT	−13.3 + 1.0	9.6 + 0.3	9	2.6	–
K525C	−41.4 + 1.6	12.6 + 1.0	6	2.0	−1.2 + 0.2
R528C	+1.0 + 1.7[d]	10.4 + 0.5	6	2.4	+0.9 + 0.1
R531C	+29.1 + 1.7[d]	9.7 + 0.3	9	2.6	+2.7 + 0.1
R534C	−25.4 + 1.0[d]	8.9 + 0.4	14	2.8	−0.9 + 0.1
R537C	−5.5 + 2.4[d]	11.4 + 1.5	6	2.2	+0.5 + 0.2
R538C	−60.0 + 1.4[d]	4.0 + 0.5	6	6.3	−8.7 + 1.0
D466C	+28.2 + 1.4[d]	16.9 + 0.5[d]	11	1.4	+1.6 + 0.1

[a]$V_{0.5}$ and k are half-maximum activation voltage and slope factor of the simple Boltzmann fit to activation curves (Fig. 2 B); normalized tail current = $1/[1 + \exp((V_{0.5} - V_t)/k)]$.

[b]z_g is gating charge estimated from the mean value of slope factor from the Boltzmann fit ($\bar{k}$), as $z_g = \bar{k}(RT/F)$, where RT/F = 25 mV.

[c]$\Delta\Delta G_o$ is mutation-induced perturbation of free energy (ΔG_o) involved in channel activation as $\Delta\Delta G_o = \Delta G_o^{MUT} - \Delta G_o^{WT}$, where ΔG_o^{MUT} and ΔG_o^{WT} are ΔG_o values of mutant and WT channels, respectively. ΔG_o is calculated as $RT(V_{0.5}/k)$, where RT = 0.592 kcal/mol, $V_{0.5}$ and k are from Boltzmann fit. Standard error was calculated as $(SEM_{MUT}^2 + SEM_{WT}^2)^{1/2}$, where SEM_{MUT} and SEM_{WT} are standard error of ΔG_o^{MUT} and ΔG_o^{WT}, respectively.

[d]One-way ANOVA, $P < 0.001$, followed by Tukey's test of multiple comparisons with WT, $P < 0.05$.

Fig. 3 A depicts current traces of WT-hERG and mutant channels recorded at different levels of V_r after channel activation and inactivation by a strong depolarization pulse to +60 mV. For each cell the peak or plateau levels of tail currents are normalized by the maximum outward tail current recorded at −50 to −30 mV, and the data are averaged over cells (current–voltage relationships shown in Fig. 3 B). In all cases, there is a prominent negative slope in the V_r range of −50 to +30 mV, i.e., smaller outward currents at more depolarization voltages. This "inward rectification" property reflects the fast and voltage-sensitive inactivation process of the hERG channel. Furthermore, except for K525C, the reversal potentials (E_{rev}) for WT and all the other mutant channels are at about −100 mV. This is close to the calculated K^+ equilibrium potential (E_K) under our recording conditions (−105 mV, assuming $[K]_i$ of 125 mM) (Dascal, 1987). Since K525C has a sizable open probability at the oocytes' resting membrane potential (Fig. 2 A), the $[K]_i$ may be lower than 125 mM, causing a positive shift of E_K to ∼−80 mV. This is supported by the observation that a total replacement of external Na^+ ions with NMDG shifts E_{rev} of K525C from −81.8 + 1.1 to −86.1 + 0.1 mV (n = 3 each), corresponding to a permeability ratio of Na^+ to K^+ of only 0.003 (calculated based on the constant field equation).

How serious is the perturbation of hERG's structure–function relationship by these single charge mutations? Mutation-induced changes in the free energy of channel activation ($\Delta\Delta G_o$) are listed Table I. The highest degree of perturbation is seen in K538C ($\Delta\Delta G_o$ = −8.7 ± 1.0 kcal/mol). This change amounts to the energy of

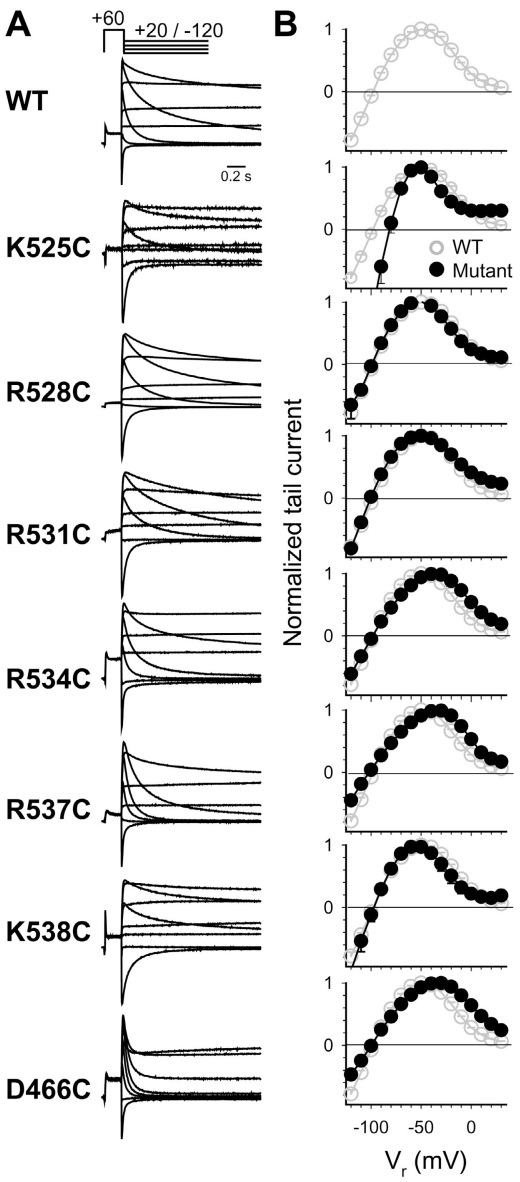

FIGURE 3. Cysteine substitutions of S4's positive charges had little effect on the inward rectification property and reversal potential of hERG. (A) Original current traces were elicited by the voltage clamp protocol diagrammed on top. From V_h −80 or −90 mV, a strong depolarization pulse to +60 mV for 0.2 s was used to activate and inactivate the channels. This was followed by repolarization pulses from +30 to −120 mV in 10-mV increments (current traces shown were from +20 to −120 mV in 20-mV steps) during which channels rapidly recovered from inactivation and then deactivated. Recordings were made in 2 mM $[K]_o$ (estimated E_K −105 mV, assuming $[K]_i$ 125 mM). (B) Current–voltage relationships from experiments as shown in A. The peak or plateau amplitudes of tail currents were normalized by the maximum outward tail current in each cell (occurring at V_r −50 to −30 mV) and averaged. Gray open circles and black circles are for WT and mutant, respectively (n = 6–14 each).

less than two H bonds in aqueous solution (4–5 kcal/mol per H bond), suggesting that the degrees of voltage shift shown in Fig. 2 B can be due to subtle changes in the channel's conformation. Fig. 3 shows that these charge mutations do not disrupt the function of the pore domain (fast inactivation process and high K^+ selectivity). Therefore, these charge mutations do not drastically alter the structure–function relationship of the hERG channel, justifying their use in the following experiments.

Effects of Charge Mutations on the Number of Equivalent Gating Charges Involved in hERG Activation

The slope factors of Boltzmann fit to activation curves can be used to calculate the number of gating charges of channel activation (z_g, Table I). Except for D466C, the z_g values of the mutant channels are similar to, or even larger than (K538C), the z_g value of WT-hERG. Since z_g values are calculated based on a simple two-state channel gating model and can be influenced by cooperative interactions between subunits, they are not sensitive or accurate enough to deduce the number of gating charges involved in the activation process. Therefore, we use a less model-dependent "limiting slope" method to estimate the number of equivalent gating charges for hERG activation (Zagotta and Aldrich, 1990, Bezanilla, 2000):

$$z_a = \lim_{P_o \to 0} kT\, dLn(P_o)/dV, \qquad (2)$$

where z_a is equivalent gating charges (in e_o) transferred during channel activation, $dLn(P_o)/dV$ is the slope of relationship between $Ln(P_o)$ and depolarization voltage V, and k and T are the Boltzmann constant and absolute temperature. This method is valid for a sequential model with one open state, where the transition rates are exponentially dependent on the voltage.

A prerequisite in using the limiting slope method to deduce the z_a value is the ability to measure very low P_o values (estimated by normalized peak tail current amplitudes, as described for Fig. 2 B). To facilitate the measurement of extremely small tail currents at negative voltages, we record tail currents in 20 mM $[K]_o$ (raising $[K]_o$ to increase single channel conductance) (Kiehn et al., 1996) and use a negative V_r of −120 mV (to increase the driving force for inward tail currents). Furthermore, two voltage clamp protocols are used. The first protocol applies 1-s pulses in 10-mV increments to sample the full range of channel activation, and thus to measure the maximum amplitude of tail current in the plateau range of channel activation. The second protocol applies long (10 s) depolarizing pulses in 2-mV increments, starting at $V_t \sim 20$ mV below the apparent activation threshold to V_t 10–20 mV above the activation threshold (based on Fig. 2). The long (10 s) depolarization duration allows P_o to fully develop at negative V_t, when channel activation is slow. The small (2 mV) steps increase the resolution of changes in P_o around the activation threshold. Fig. 4 A depicts WT current traces elicited by these two voltage clamp protocols. Under these conditions, we can detect P_o values at 10^{-3} or even lower for WT-hERG and mutant channels.

In Fig. 4 B, the P_o values are plotted on a logarithmic scale against V_t for WT (gray open circles) and mutant channels (black open circles). Data are averaged from three to six measurements each. For each measurement, the relationship between $Ln(P_o)$ and V_t is subjected to linear regression analysis to estimate the slope at the lower limit of P_o. This slope is then used to calculate z_a according to Eq. 2. The results for WT-hERG and mutant channels are plotted in Fig. 4 C. Neutralizing the first three positive charges in S4 (K525C, R528C, and R531C) and the negative charge in S2 (D466C) reduces z_a, supporting their role as "gating charges" for hERG activation. On the other hand, neutralizing the inner three positive charges in S4 (R534C, R537C, and K538C) has no effect on z_a.

MTSET Accessibility Test of Cysteine Side Chains Introduced Into Charged-residue Positions in S4 and S2

If a charge is within the membrane electrical field and thus capable of sensing changes in the membrane voltage, its position relative to the membrane barrier will change during channel gating. Cysteine introduced into its position is expected to change the thiol side chain accessibility to the surrounding aqueous crevice in a state-dependent manner (assuming that the cysteine substitution does not alter the native side chain orientation) (Wang et al., 1999). On the other hand, charged residues not involved in gating charge transfer do not change their positions relative to the membrane barrier. Their side chain accessibility to the aqueous crevice should not be state dependent. Therefore, to confirm the role of the first three positive charges in S4 and D466 in S2 as the "gating charges" in hERG's activation process, we test the accessibility of introduced cysteine side chains to extracellular and intracellular MTSET ($MTSET_o$ and $MTSET_i$). Ideally, accessibility to $MTSET_i$ should be tested using the inside-out patch recording configuration and applying MTSET directly to the intracellular side of the membrane (Baker et al., 1998, Bell et al., 2004). Unfortunately, due to the low expression level of cysteine mutants in oocytes (in 2 mM $[K]_o$ maximal whole cell outward currents <10 μA), it is difficult to record large and stable currents from inside-out patches. Thus, we take an alternative approach: applying $MTSET_i$ using intra-oocyte injection.

Neither $MTSET_o$ nor $MTSET_i$ Affects the WT hERG Channel. There are 24 native cysteines in WT hERG. Previously, we have shown that $MTSET_o$ (1 mM) has no ef-

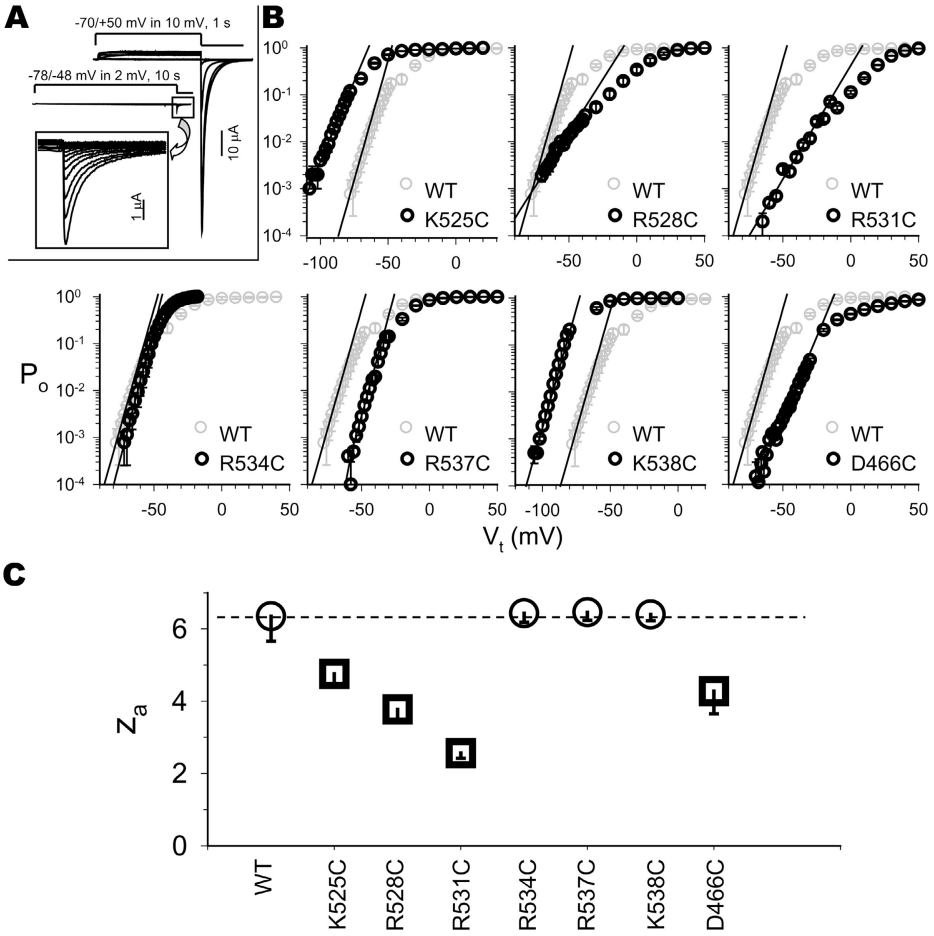

FIGURE 4. Estimating the number of equivalent gating charges involved in channel activation (z_a) using the limiting slope method. (A) Original current traces of WT-hERG recorded in 20 mM $[K]_o$. Tail currents (measured at −120 mV) were elicited by two protocols. (1) 1-s pulses were applied in 10-mV increments to V_t covering the whole voltage range of channel activation (based on Fig. 2 B). These are illustrated by the top family of current traces. (2) For a V_t range from below the activation threshold to ~20 mV above the threshold, long (10-s) pulses were applied in 2-mV increments to gain a high resolution analysis of increase in channel open probability (P_o) at V_t around the activation threshold. These are illustrated by the middle family of current traces, with the boxed area enlarged in the bottom family of current traces. The 10 μA calibration applies to the top and middle families of current traces, and the 1 μA calibration applies to the bottom family of current traces depicted in the box. The peak amplitudes of tail currents were normalized by the maximum tail current following the most depolarized V_t to estimate P_o at the end of preceding depolarizing pulses. The same recording conditions and similar voltage clamp protocol were used for all the mutant channels, with V_t levels adjusted depending on the voltage range of activation. (B) P_o values are plotted on a logarithmic scale against V_t for WT (gray open circles) and mutants (black open circles, mutant type specified in each panel). The relationships between $Ln(P_o)$ and V_t were subjected to linear regression analysis to estimate the limiting slope at low P_o levels ($P_o \sim 10^{-3}$). The value of z_a was calculated according to z_a = slope*(RT/F), where RT/F = 25 mV. The lines superimposed on the data points are calculations based on the mean limiting slopes. (C) Summary of z_a for WT and mutant channels (n = 3–6 each, mean + SEM).

fects on WT hERG (Fan et al., 1999). Fig. 5 shows that $MTSET_i$ (estimated initial cytoplasmic concentration 2 mM) does not affect WT hERG either. The efficacy of intra-oocyte injection is confirmed by the observation that injecting TEA (estimated cytoplasmic concentration 2 mM) causes a prominent decrease in the WT hERG current amplitude (Smith et al., 1996). These data indicate that either native cysteines in hERG are not accessible to $MTSET_o$ and $MTSET_i$ or their modification by MTSET has no impact on channel function. Therefore, the effects of $MTSET_o$ and $MTSET_i$ on cysteine-substituted mutants can be attributed to modification of the introduced cysteine side chains.

Cysteine Side Chain at 525 is Accessible to $MTSET_o$ in a State-dependent Manner but Inaccessible to $MTSET_i$. The most prominent effect of K525C modification by MTSET is a slowing of channel deactivation. Therefore, we use the half-time ($T_{1/2}$) of decay of tail current at −120 mV to quantify the degree of K525C modification by MTSET. Three protocols are used to evaluate the state dependence of K525C modification by $MTSET_o$. $MTSET_o$ is applied (1) while the oocyte membrane is held at V_h −80 mV to keep most of the channels in the closed states (Fig. 6 A), (2) while the membrane is held at 0 mV to keep the channels in the open/inactivated states (Fig. 6 B), or (3) while the membrane voltage is pulsing from V_h −90 mV to +40 mV for 1 s once every 30 s to cycle the channels between closed and open/inactivated states (Fig. 6 C). For the first two protocols, $MTSET_o$ (1 mM) is applied for 5 min (flow rate 5–6 ml/min, bath solution totally exchanged in <30 s), and the effect on $T_{1/2}$ of channel deactivation is measured after 5 min washout of $MTSET_o$. Fig. 6 B shows that applying $MTSET_o$ while holding the channels in open/inactivated states allows K525C modification by MTSET; $T_{1/2}$ is markedly prolonged to 4.2 ± 0.7 of control (n = 8). Fig. 6 A shows that applying $MTSET_o$ while holding the channels in the closed state prevents K525C modifi-

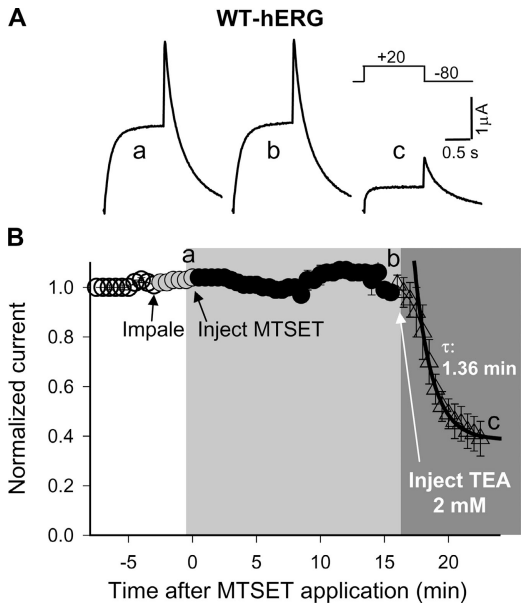

FIGURE 5. Efficacy of intracellular application of hydrophilic reagents using the oocyte injection device during voltage clamp. (A) Original current traces recorded from an experiment on WT hERG at time points a, b, and c corresponding to those denoted along the time course in B. (B) Average time course of changes in WT-hERG peak tail current amplitude ($n = 4$). Current was elicited by 1-s depolarization pulses to +20 mV once every 30 s and tail current was recorded at −80 mV. After control data were obtained, the oocyte was impaled with a fine-tipped injecting pipette filled with MTSET (100 mM) solution (impale, gray symbols). After confirming current stability, MTSET was injected (10 nl, estimated cytoplasmic concentration = 2 mM, assuming oocyte volume = 0.5 μl, black symbols/light gray shade). 10 min after MTSET injection, the injecting pipette was pulled out, refilled with TEA (100 mM) solution, and reimpaled into the oocyte. TEA was injected as described above (10 nl, cytoplasmic concentration = 2 mM, open triangles/dark gray shade). The curve superimposed on the open triangle data points after the initial sigmoid phase represents single exponential fit to the mean time course of WT-hERG suppression by TEA_i, with time constant (τ) marked.

cation by MTSET ($n = 4$). Using the third protocol, $MTSET_o$ exposure causes a gradual slowing of K525C deactivation ($T_{1/2}$ prolonged to 2.4 ± 0.2 of control, $n = 7$). Since K525C modification by $MTSET_o$ occurs in the open/inactivated state, the cumulative exposure time to $MTSET_o$ in the open/inactivated state can be calculated (additional abscissa below the data points during $MTSET_o$ exposure in Fig. 6 C). The time course of K525C modification by $MTSET_o$ can be well described by a single exponential function. The τ value is 4 mM·s, which translates into a modification rate of 250 $M^{-1}s^{-1}$. Note that $T_{1/2}$ prolongation after exposure of K525C to $MTSET_o$ at V_h 0 mV is not sustained, but gradually declines (to 3.2 ± 0.4 of control at steady state, $n = 8$). This degree of $T_{1/2}$ prolongation is not statistically different from that reached when $MTSET_o$ is applied during constant pulsing ($P = 0.106$). This suggests that some of the 525C residues might have lost their MTSET adduct when the channels cycle through the closed–open states, perhaps because the gating pore around S4 is too narrow for the MTSET-modified 525C side chain to go through easily.

Fig. 6 D shows that MTSET applied to the cytoplasmic side of the cell membrane does not affect the K525C tail kinetics even after a 20-min exposure. After MTSET injection, extracellular application of $MTSET_o$ induces a marked prolongation of tail current, supporting the modifiability of the K525C side chain. Similar observation was obtained in five experiments.

Cysteine Side Chains Introduced into the Other Positive-charge Positions in S4 Are Accessible to $MTSET_i$ but not to $MTSET_o$. Fig. 7 summarizes the MTSET accessibility of cysteine side chains introduced into the other five positive-charge positions in S4: R528C, R531C, R534C, R537C, and K538C. The major effect of MTSET modification on these mutant channels is a suppression of current amplitude (Fig. 7 B, insets). Therefore, we use the decrease in the peak tail current amplitude as a measure of MTSET modification of introduced cysteine side chains at these positions.

The left panel of Fig. 7 A shows $MTSET_o$ application to R528C for 5 min while the membrane voltage is held at +20 mV (reaching an average of 80% channel activation, Fig. 2 B, or a total exposure time of 528C to $MTSET_o$ in the open/inactivated state of 240 mM·s). There is no sign of R528C modification by $MTSET_o$ under this condition. The remaining four panels of Fig. 7 A depict time courses of changes in the peak tail current amplitudes of R531C, R534C, R537C, and K538C before, during, and after $MTSET_o$ (1 mM) exposure ($n = 4$–7 each). $MTSET_o$ does not affect these mutant channels. These observations indicate that cysteine side chains introduced into these five positions in S4 are not accessible to $MTSET_o$.

For all the five cysteine mutants, applying MTSET to the cytoplasmic side of the cell membrane causes a gradual decrease in the current amplitude, indicating that cysteine side chains at all five positions are accessible to $MTSET_i$ (Fig. 7 B). The state dependence of $MTSET_i$ accessibility is tested by comparing the degree of current reduction when $MTSET_i$ is applied under two voltage clamp protocols. For the first protocol, MTSET is injected into the oocyte while the membrane voltage is held at −80 mV with only brief (0.5 s) depolarization pulses applied once every 30 s to monitor the degree of current reduction ("closed state–preferred" exposure, represented by solid circles). For the second protocol, MTSET is injected into the oocyte while the membrane is held at a depolarized V_t for 20 s using a duty cycle of 30 s ("open/inactivated state–preferred" exposure, represented by open circles, details in Fig. 7 legend). For each of the mutant channels, the average time courses

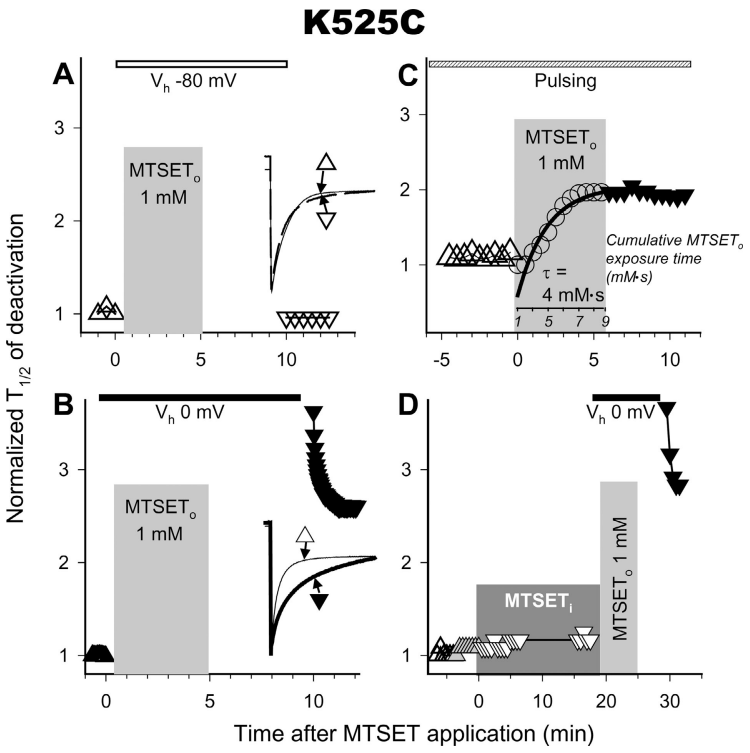

FIGURE 6. Sidedness and voltage dependence of MTSET accessibility to cysteine side chain introduced into position 525. (A–C) Effects of $MTSET_o$ on K525C depended on the voltage clamp protocol during $MTSET_o$ application. Shown in each panel is a time course of changes in the half-time ($T_{1/2}$) of K525C deactivation measured at −120 mV. In A and B, the membrane voltage was held at a constant V_h (−80 or 0 mV, denoted by the horizontal bars) for 10 min. $MTSET_o$ 1 mM was applied during the first 5 min (denoted by gray shades) and washed out for 5 min. Afterwards, the V_h was returned to −90 mV and the pulsing was resumed to monitor the deactivation kinetics. Insets, K525C tail currents recorded before (thin solid traces) and after (dashed trace or thick solid trace) $MTSET_o$ treatment. In C, the membrane was constantly pulsing from V_h −90 to +40 mV for 1 s once every 30 s before, during (gray shade), and after $MTSET_o$ exposure. The additional horizontal axis for data points during $MTSET_o$ exposure denotes the cumulative open-state exposure (1-s exposure to 1 mM $MTSET_o$ at +40 mV once every 30 s). The curve superimposed on the data points represents single exponential fit with τ = 4 mM·s. (D) Time course of changes in $T_{1/2}$ of K525C deactivation when the oocyte was impaled and injected with MTSET ($MTSET_i$ 2 mM, dark gray shade). 18 min after MTSET injection, the membrane voltage was held at 0 mV for 10 min (denoted by the black horizontal bar), during which the oocyte was exposed to $MTSET_o$ 1 mM for the first 5 min (light gray shade) followed by wash out for 5 min. The tail current deactivation rate after $MTSET_o$ treatment was monitored. In all panels, the coordinates are $T_{1/2}$ values normalized to the control values, and the abscissas are time after MTSET application to the bath (A–C) or into the oocyte (D).

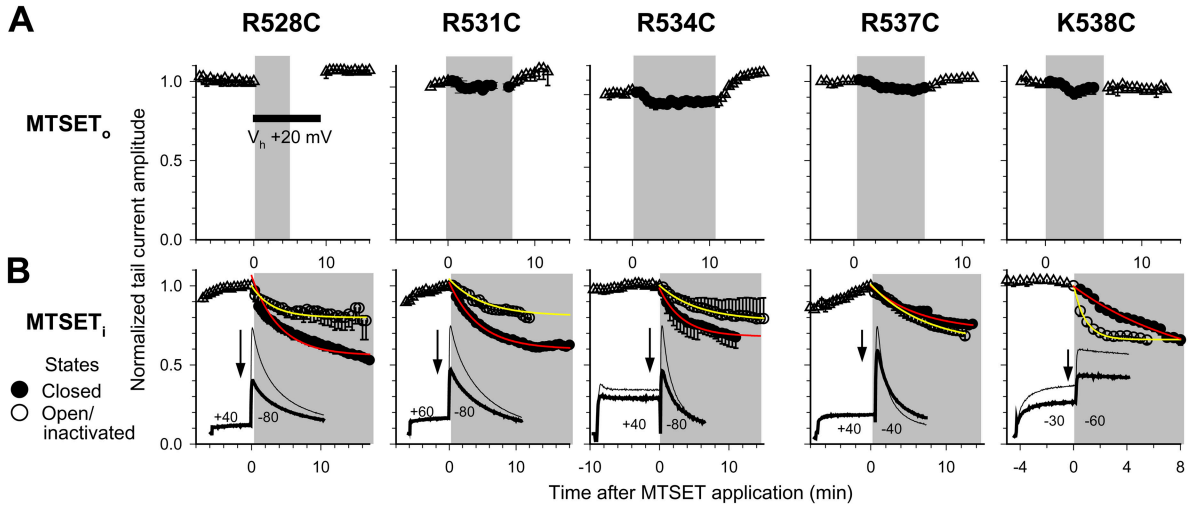

FIGURE 7. Sidedness and state dependence of MTSET accessibility to cysteine side chains introduced into positions 528, 531, 534, 537, and 538 (mutant types marked on top). For each channel, the top graph (A) is an average time course of changes in current amplitude before, during (gray shades), and after exposure to extracellular MTSET (1 mM). For R528C, the membrane voltage was held at +20 mV for 10 min and $MTSET_o$ was applied during the first 5 min and then washed out for 5 min. For the other mutants, the membrane was pulsing from V_h (−80 mV for all, except K538C, V_h = −90 mV) to V_t (as specified in the insets of lower graphs) for 1 s every 30 s. The solid circles during $MTSET_o$ exposure denote closed state–preferred exposure because the channels spent 29 s of the 30-s cycle in the closed states. The bottom graphs (B) show the average time courses of current amplitude before (open triangles) and after intracellular injection of MTSET (estimated initial cytoplasmic concentration 2 mM, gray shades). The closed circles denote closed state–preferred exposure; channels stayed in the closed states at V_h −80 or −90 mV and only activated by 0.5-s test pulses to V_t (as denoted in the insets) once every 30 s. The open circles denote open/inactivated state –preferred exposure; channels stayed in open/inactivated states for 20 s at denoted V_t and only spend 10 s back to V_h once every 30 s. The curves superimposed on the data points are single exponential fits. Insets, original current traces before (thin traces) and 8–16 min after $MTSET_i$ injection using the closed state–preferred exposure protocol (thick traces). Arrows indicate the changes in peak tail current amplitudes.

of $MTSET_i$ modification using these two protocols are plotted in the same graph to facilitate comparison (n = 3–8 each). When $MTSET_i$ is applied using the closed state–preferred exposure protocol, the current amplitude gradually declines following an apparent single exponential time course. The time constants are 5.6 min (R528C), 4.5 min (R531C), 3.3 min (R534C), 6.6 min (R537C), and 8.9 min (K538C). On the other hand, when $MTSET_i$ is applied using the open/inactivated state–preferred exposure, the degree of $MTSET_i$ modification is significantly reduced for R528C and R531C ($P < 0.05$ for data points following the first 2 min after MTSET injection). The observation that the apparent degree, instead of the rate, of current suppression by $MTSET_i$ is state dependent may be explained by (a) MTSET hydrolysis by the reducing environment of oocyte cytoplasm, and (b) slow rates of $MTSET_i$ modification of 528C and 531C. There is no statistically significant difference in R534C or R537C modification by $MTSET_i$ between the closed and open/inactivated state–preferred exposures. $MTSET_i$ modification of K538C proceeds more rapidly when $MTSET_i$ is applied using the open/inactivated state–preferred exposure than using the closed state–preferred exposure.

Cysteine Side Chain at Position 466 in S2 Is Accessible to $MTSET_o$ in a State-dependent Manner. Previously we showed that 466C is accessible to $MTSET_o$, and the accessibility is higher when the channel is in the closed state than in the open/inactivated states (Liu et al., 2003). We now test whether 466C is accessible to $MTSET_i$ and whether this accessibility manifests a state dependence opposite to that of $MTSET_o$ accessibility. Fig. 8 (A and B) shows two representative time courses of change in D466C current amplitude (measured by the peak tail currents at −60 mV, insets) before and after impalement with a pipette containing 100 mM MTSET solution, and after $MTSET_i$ injection (estimated initial cytoplasmic concentration 2 mM). The membrane voltage is cycling through open/inactivated states (1 s to +60 mV, once every 30 s) and the closed state (V_h −80 mV). There is a very gradual and modest reduction in the D466C current amplitude (by ~20% after 15 min exposure). On the other hand, when the oocyte is subsequently exposed to 1 mM $MTSET_o$ for 5 min while the membrane is held at −80 mV (closed state–preferred exposure) and then washed out, the D466C current is practically abolished (Fig. 8 A). In Fig. 8 B, the oocyte is exposed to 1 mM $MTSET_o$ for 5 min while the membrane is held at +20 mV (open/inactivated state–preferred exposure) followed by washout, there is a further but very modest modification of D466C by $MTSET_o$. Similar observations are obtained in five experiments. These data confirm that D466C is more accessible to $MTSET_o$ in the closed state than in the open/inactivated states. However, D466C has only limited ac-

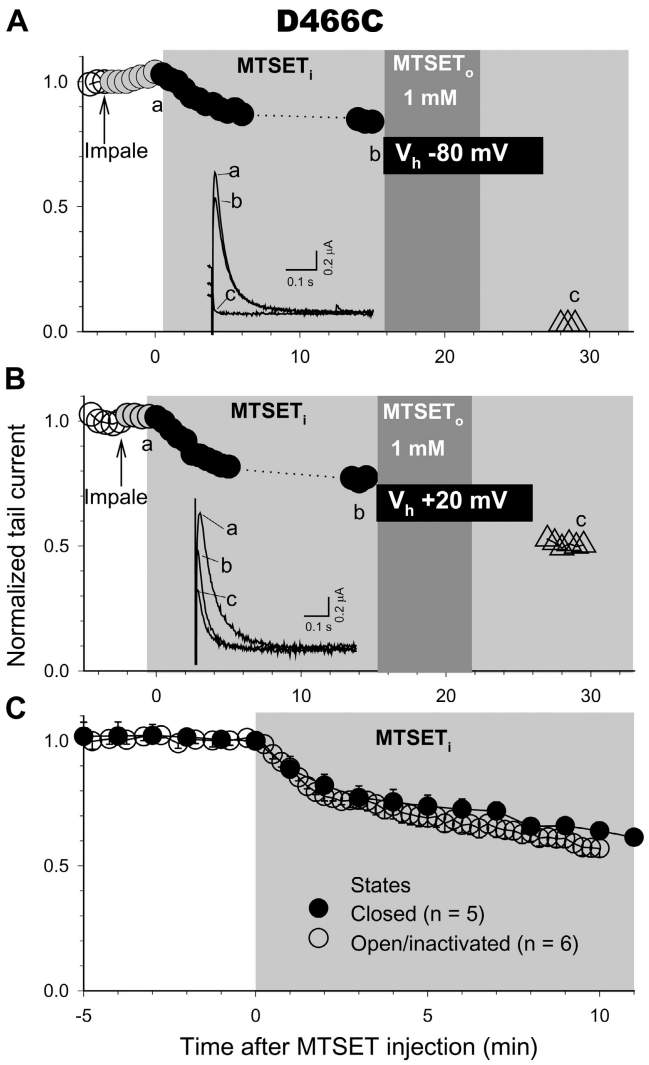

FIGURE 8. Accessibility of cysteine side chain introduced into position 466 in S2 to $MTSET_i$ and $MTSET_o$. (A and B) Time courses of changes in D466C peak tail current amplitude (elicited by 1-s pulse to +60 mV followed by repolarization to −60 mV) normalized to the control amplitude (open circles). Gray circles indicated data points after impalement with an injecting pipette. Black circles denote data points after MTSET injection (estimated initial cytoplasmic concentration 2 mM). Approximately 15 min after injection and in the continuous presence of intracellular MTSET (light gray shade), membrane voltage was held at −80 (A) or +20 (B) mV for 10 min (black horizontal boxes), during which the oocytes were exposed to 1 mM $MTSET_o$ for the first 5 min (dark gray shade) followed by washout. Open triangles depict data points after the washout of $MTSET_o$. Insets, superimposed tail currents recorded from the same experiments as shown in the main graphs at time points a–c. (C) Time course of changes in D466C tail current amplitude in response to $MTSET_i$ (estimated initial concentration 2 mM). To test whether 466C modification by $MTSET_i$ was state dependent, two voltage clamp protocols were used: (1) closed state–preferred $MTSET_i$ exposure, short (0.5 s) depolarization pulses to +40 mV applied once every 60 s, and (2) open/inactivated state–preferred exposure, long (10 s) depolarization pulses to +40 mV applied once every 15 s. Data were averaged from five and six experiments, respectively.

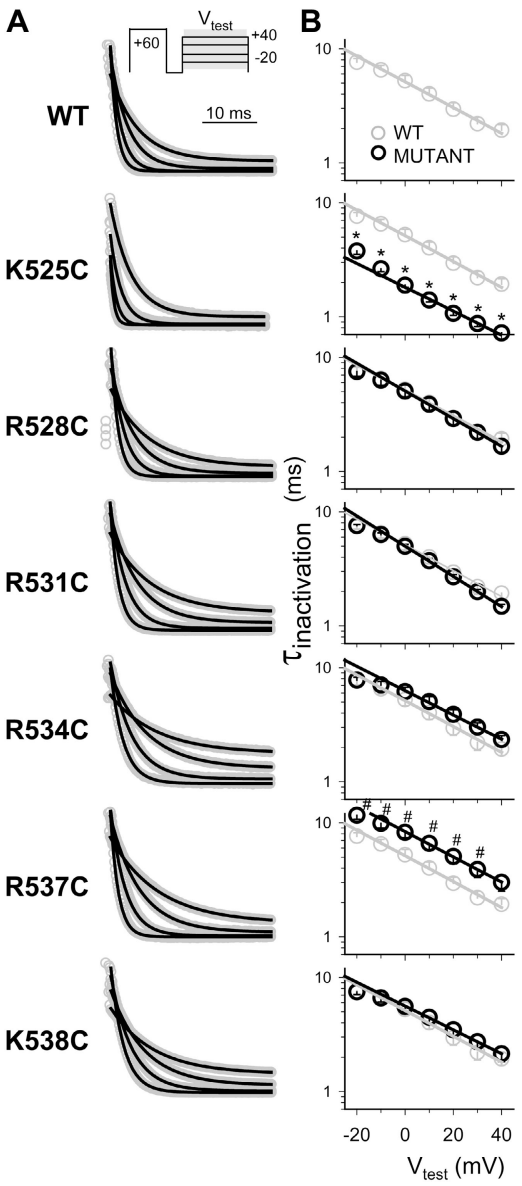

FIGURE 9. Effects of cysteine substitution of S4's positive charges on the kinetics and voltage dependence of fast inactivation in the hERG channel. (A) Original current traces elicited by the voltage clamp protocol diagrammed on top; 0.2-s depolarizing pulse to +60 mV (except R531C for which depolarization was to +80 or +100 mV) was used to activate and then inactivate the channels. This was followed by a short repolarizing pulse (15 ms to −80 mV) to allow channels to recover from inactivation without significant deactivation. The membrane voltage was then depolarized to V_{test} ranging from +40 to −20 mV in 10-mV increments, during which channels reinactivated. The time course of reinactivation could be well described by a single exponential function. Shown are current data (as gray circles), superimposed with the fitted single exponential function (black traces). (B) Summary of time constants (τ) of inactivation. Values of $\tau_{inactivation}$ are plotted on a logarithmic scale. The relationship between $Ln(1/\tau_{inactivation})$ and V_{test} was subject to linear regression analysis to estimate the slope. The slope is used to calculate z_i, according to Eq. 3 in the text. *, $P < 0.001$ K525C vs. WT; #, $P < 0.05$ R537C vs. WT. Experiments were done in 2 mM $[K]_o$.

cessibility to $MTSET_i$ with no clear state dependence (Fig. 8 C).

Effects of S4 Charge Mutations on the Voltage Sensitivity of hERG's Inactivation Process

Fig. 3 shows that there are no major changes in the degree of hERG inactivation when S4's positive charges are substituted by cysteine individually. We further quantify the voltage sensitivity of inactivation in WT hERG and the cysteine mutants. A triple-pulse protocol is used to estimate the rate of channel inactivation at different voltages (Fig. 9 A, top). A long and strong depolarizing pulse to +60 mV (+80 or +100 mV for R531C) fully activates and inactivates the channels. This is followed by a short repolarizing step to −80 mV for 15 ms, during which the inactivated channels recover from inactivation ($\tau \sim 3$ ms) without appreciable deactivation (the fast and slow time constants of deactivation range 20–100 and 200–1,000 ms, respectively, at −80 mV; unpublished data). The membrane is then stepped to test voltages ranging from +40 to −20 mV, during which the channels reinactivate. For WT and mutant channels, this process can be well described by a single exponential function, as is shown by the curve fitting to representative current traces in Fig. 9 A. The values of $\tau_{inactivation}$ are plotted on a semilogarithmic scale versus the test voltages (V_{test}) in Fig. 9 B. A linear regression analysis of the reciprocal of $\tau_{inactivation}$ vs. V_{test} gives an estimate of the gating charge involved in the inactivation process according to Eq. 3.

$$K(V_{test}) = K(0)\exp[z_i V_{test}(F/RT)] \quad (3)$$

or

$$Ln[K(V_{test})] = Ln[K(0)] + z_i V_{test}(F/RT),$$

where $K(V_{test})$ and $K(0)$ are the rate constants of inactivation (reciprocal of $\tau_{inactivation}$) at voltages V_{test} and 0 mV, respectively, and $F/RT = 0.04\ mV^{-1}$. The values of z_i are listed in Table II. These charge mutations do not have statistically significant effects on the z_i value (ANOVA, $P > 0.05$). The rate of K525C inactivation is significantly faster than that of WT (Fig. 9 B). Although $MTSET_o$ modification of 525C greatly slows the rate of deactivation (Fig. 6), this intervention has no effect on K525C inactivation (unpublished data), further supporting the notion that this S4 positive charge is not involved in channel inactivation.

DISCUSSION

The major findings in this study can be summarized as the following. (a) The number of gating charges transferred during hERG activation (z_a) is estimated to be

TABLE II

Equivalent Gating Charges Estimated for the Activation and Inactivation Gating Processes of WT hERG and Mutant Channels

Channel	z_a[a]	*n*	z_{total}[b]	z_i[c]	*n*
	e_o		e_o	e_o	
WT	6.35 + 0.69	5	8	0.72 + 0.03	11
K525C	4.76 + 0.36	5	6	0.61 + 0.05	11
R528C	3.77 + 0.35[d]	6	4.7	0.71 + 0.03	7
R531C	2.56 + 0.14[d]	5	3.2	0.76 + 0.01	10
R534C	6.43 + 0.25	6	8	0.61 + 0.01	11
R537C	6.46 + 0.22	4	8.1	0.67 + 0.04	7
K538C	6.40 + 0.18	4	8	0.62 + 0.05	5
D466C	4.28 + 0.63	3	5.4	0.75 + 0.10	5

n, number of experiments.

[a]z_a is the number of equivalent gating charges involved in channel activation estimated by the limiting slope method.

[b]z_{total} is the number of total gating charges estimated from the mean value of z_a ($\bar{z}_a$) as $\bar{z}_a/0.8$, assuming that when measured at $P_o = 10^{-3}$, the z_a value underestimates z_{total} by 20% (Schoppa et al., 1992; Zagotta et al., 1994).

[c]z_i is the number of equivalent gating charges involved in channel inactivation, determined based on data shown in Fig. 9 B. The relationship between $Ln(1/\tau_{inactivation})$ and V_{test}, where $\tau_{inactivation}$ is time constant of inactivation determined at V_{test} (+40 to −20 mV), is subject to linear regression to estimate the slope, and the z_i value is calculated as slope(RT/F), according to Eq. 3 in text.

[d]One-way ANOVA, $P < 0.001$, followed by Dunn's multiple comparison with WT, $P < 0.05$.

6.4, based on the limiting slope method. (b) Neutralizing the first three positive charges in hERG's S4 segment reduces z_a while neutralizing the following three positive charges does not, suggesting that the first three positive charges are involved in gating charge transfer. (c) Consistent with the above observations, cysteine side chains introduced into the first three, but not the following three, positive-charge positions in S4 manifest state-dependent changes in their MTSET accessibility, consistent with an outward S4 movement relative to the membrane barrier during depolarization. (d) Neutralizing D466 in S2 reduces z_a. Furthermore, cysteine side chain at 466 manifests a state-dependent change in $MTSET_o$ accessibility, consistent with an inward S2 movement relative to the membrane barrier during depolarization. (e) None of the charge mutations affect the number of gating charges involved in hERG's inactivation process (z_i).

Comparison Between hERG and Shaker of Scheme of Gating Charge Transfer During Channel Activation

Based on the "conventional gating model" that results from extensive studies on the Shaker channel (Baker et al., 1998; Bezanilla, 2000; Cohen et al., 2003; Horn, 2004; Starace and Bezanilla, 2004), the S4 is oriented more or less perpendicular to the plane of the cell membrane, contacting the periphery of the pore domain on one side, and surrounded by S1, S2, and S3 on the other. Most of the S4's surface is exposed to water-filled crevices connected to the extracellular or intracellular aqueous compartment, where the positive charges on S4 are stabilized by negative charges on S1, S2, or S3, and by counter ions in the crevices. Only a narrow portion of the S4 is in a "gating pore," which forms a barrier between the extracellular and intracellular compartments where the membrane electrical field is focused. Membrane depolarization exerts an electrostatic force on S4's positive charges that are within or near the membrane electrical field and thus can sense changes in the membrane voltage (gating charges). This causes S4 movements, resulting in a transfer of gating charges through the gating pore. The other positive charges on the S4 that cannot sense the membrane voltage are not involved in gating charge transfer, but can serve other functions (e.g., producing topogenic signals during folding of nascent channel proteins) (Papazian et al., 2002). In the Shaker channel, the first four positive charges carry gating charges: R362, R365, R368, and R371 (Starace and Bezanilla, 2004). In addition, a negative charge in the cytoplasmic half of S2 (E293, Fig. 1 D) may also contribute to the gating charges (Seoh et al., 1996).

Table II lists the equivalent gating charges (z_a, in e_o) for WT hERG and cysteine-substituted mutants. It has been shown that z_a values obtained by the limiting slope method underestimate the total numbers of gating charges (z_{total}) by ~20% (Schoppa et al., 1992; Zagotta et al., 1994). Therefore, we further estimate the z_{total} values of WT-hERG and mutant channels using the mean values of z_a: $z_{total} = z_a/0.8$. The values of z_{total} are also listed in Table II.

Our data support the alignment of S4's positive charges between hERG and Shaker shown in Fig. 1 B (also shown in Fig. 10, top). (a) The first three positive charges in hERG's S4 carry gating charges during channel activation. (b) The z_{total} for WT hERG is ~8 e_o, less than that of the Shaker channel (12–13 e_o) by 4–5 e_o (Schoppa et al., 1992; Aggarwal and MacKinnon, 1996; Seoh et al., 1996). This difference is consistent with the notion that hERG has one less gating charge per subunit that traverses most of the membrane electrical field during activation. The first positive charge in Shaker's S4, R362, fulfills this criterion (Aggarwal and MacKinnon, 1996). (c) The pattern of state dependence of MTSET accessibility of cysteine side chains introduced into the S4 segment of the hERG channel is in general agreement with that described for the equivalent positions in the Shaker channel (Fig. 10) (Larsson et al., 1996; Baker et al., 1998). Furthermore, our data support a role of D466 in S2 in gating charge transfer, again similar to the putative role of E293 in S2 of the Shaker channel (Seoh et al., 1996). Thus the scheme of gating charge transfer during the activation process is similar between hERG and Shaker.

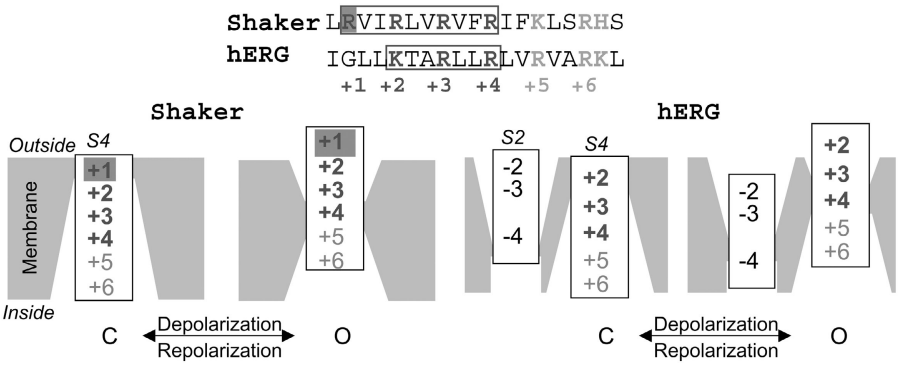

FIGURE 10. (Top) Alignment of S4 amino acid sequences of Shaker and hERG. The positive charges are denoted by generic numbers below. Boxes highlight voltage-sensing (gating) charges in each channel. Gray shade highlights the Shaker arginine that is absent in hERG. (Bottom) Diagrams illustrating putative movements of Shaker's S4 and hERG's S2 and S4, relative to the membrane barrier, during channel activation. The Shaker diagram is based on (Starace and Bezanilla, 2004), with the first four positive charges switched from internally exposed positions in closed states to externally exposed in the open states. Although E293 in the Shaker S2 may contribute to gating charge transfer, it is not included in the diagram because there is no data on the accessibility of 293C to $MTSET_o$ or $MTSET_i$. The hERG diagram is based on data from the present study, with one exception. Although we cannot detect any $MTSET_o$ accessibility of 528C (+3 in the diagram) in the open state, this side chain is accessible to external *p*-chloromercuibenzene sulfonate (pCMB, a smaller thiol-modifying reagent than MTSET) in the open state (Mitcheson, J.S., personal communication). The crevice around S2 is deep in the hERG channel, so that cysteine side chain at position −3 is readily accessible to extracellular $MTSET_o$ (Liu et al., 2003). Cysteine at position −4 (466C) is accessible to $MTSET_o$ in the closed state but not in the open state. $MTSET_i$ also modifies 466C, although the effect is much less than that of $MTSET_o$ in the closed state, and there is no clear state dependence in $MTSET_i$ modification of 466C. These observation are depicted by a narrow inwardly accessible crevice around S2 at the −4 level in both closed and open states.

The state dependence of 528C and 531C accessibility to $MTSET_i$ is qualitatively similar to that described for the equivalent positions in the Shaker channel, 368C and 370C (Larsson et al., 1996; Baker et al., 1998). However, quantitatively the change in modification rate in hERG (open to closed state transition increases the $MTSET_i$ modification rate of 528C and 531C by 4- and 1.5-fold, respectively) is much less than that seen in Shaker (open to closed state transition increases the $MTSET_i$ modification rate of 368C and 370C by 100- and 10-fold). This suggests structural differences between hERG and Shaker. Perhaps the inner crevice around S4 is narrower in hERG than in Shaker, restricting $MTSET_i$ accessibility to cysteine side chains at these positions even in the closed state.

Why Is the Activation Process in the hERG Channel So Slow?

Despite the similarity in the scheme of gating charge transfer between the two channels, the rate of hERG activation is >30-fold slower than that of Shaker. Slow activation can be due to slow movement of the voltage sensor, inefficient coupling between the voltage sensor and the activation gate, slow opening of the activation gate, or a combination of the above. Two studies suggest that a slow movement of the voltage sensor is the major cause for the slow rate of activation in the hERG channel. First, Smith and Yellen (2002) used the technique of voltage clamp fluorometry to probe conformational changes at or around the outer end of hERG's S4 in response to changes in membrane voltage. They observed a fast and a slow component of changes in fluorescence (ΔF) at positions 518 and 519, and a slow ΔF at 520. The slow ΔF is correlated with the activation and deactivation processes in terms of kinetics, voltage dependence, and sensitivity to an NH_2-terminal truncation mutation. Second, Piper et al. (2003) directly recorded gating currents (I_g) from the hERG channel. They also observed a fast and a slow component of I_g, and the slow I_g is associated with channel activation and deactivation. An S4 segment with fewer gating charges will be less sensitive to membrane depolarization, and thus may move more slowly than an S4 with more gating charges (Logothetis et al., 1992; Islas and Sigworth, 1999; Ahern and Horn, 2004). Thus, relative to the Shaker channel, the fewer gating charges in the S4 segments of hERG may contribute to reduced voltage sensitivity and a slower rate of activation.

However, other factors may also contribute to slowing the S4 movement in hERG. Negative charges in the other transmembrane segments (S1, S2, and S3) of the voltage-sensing domain may slow down S4 movement by two mechanisms. First, they may form salt bridges with S4's positive charges preferentially in the closed states (Papazian et al., 2002; Silverman et al., 2003). Our unpublished data suggest that in the hERG channel, negative charges in S1 and S2 may form salt bridges with positive charges at the two ends of S4 in the closed state (D411-K538 and D456-K525). These salt bridges can stabilize the hERG channel in the closed state and retard activation. This is consistent with the observations shown in Fig. 2 that neutralizing K525 or K538 leads to a hyperpolarizing shift in the voltage dependence of activation, which can be explained by a destabilizing effect on the closed state relative to the open state. Second, the extra negative charges in the voltage-sensing domain of hERG may

form a divalent cation (M^{2+}) binding site in the external crevice around S4, similar to that described for the EAG channels (Silverman et al., 2000; Schonherr et al., 2002). $Ca^{2+}{}_o$ or $Mg^{2+}{}_o$ bound here can restrict S4 outward movement and slow activation (more discussion below).

Where Is the Voltage Sensor for hERG's Inactivation Process?

The fast ΔF signals in the voltage clamp fluorometry experiments on hERG (Smith and Yellen, 2002) and the fast I_g component in the hERG's gating current (Piper et al., 2003) are similar in their kinetics and voltage dependence, suggesting that they originate from the same gating charge movement. This fast gating charge movement correlates well with the fast inactivation process of the hERG channel in terms of kinetics and voltage dependence. However, perturbing the fast inactivation process of the hERG channel, by mutating residues at the external pore entrance (G628C/S631C and S631A) or by applying external TEA (that interferes with conformational changes around the outer mouth), does not impact on the fast ΔF signals or the fast I_g component (Smith and Yellen, 2002; Piper et al., 2003). These suggest that the inactivation voltage sensor is well insulated from the inactivation gate at the outer mouth of the hERG channel (Smith et al., 1996; Herzberg et al., 1998). Where is this inactivation voltage sensor? Based on data from alanine scanning mutagenesis experiments on hERG's S4 segment, Tristani-Firouzi (2004) proposed that S4 is the voltage sensor for the inactivation process. On the other hand, based on the differential effects of changing $[Ca^{2+}]_o$ on the activation and inactivation processes, Johnson et al. (1999) proposed that the inactivation process has a separate voltage sensor than S4, although no specific structural elements were identified.

Our data do not support a role of S4 as the voltage sensor for hERG's inactivation process. First, neutralizing positive charges in hERG's S4 segment does not alter the gating charge mediating inactivation (z_i), although mutating the first three positive charges in S4 reduces the gating charges mediating activation (z_a) as expected. Note that our measurement of z_i, based on the voltage dependence of $\tau_{inactivation}$, matches the gating charge estimated from the fast ΔF and fast I_g experiments ($z_i \sim 0.7$). Second, the $\tau_{inactivation}$ and thus the z_i value are measured when the S4 segment is maintained at its outermost (activated) position (triple-pulse protocol in Fig. 9), and the voltage dependence of $\tau_{inactivation}$ is observed in a voltage range when channels are fully activated. Therefore, z_i cannot arise from the S4 movement that mediates channel activation.

What are the alternatives for hERG's inactivation voltage sensor? The structural element must fulfill two criteria: it must move rapidly in response to changes in membrane voltage, and it must carry only small amount of gating charge (~0.7 e_o per channel). This small gating charge can originate from negative charges in S1, S2, or S3, or from an α-helix dipole in the membrane electrical field (Bezanilla, 2000). The first possibility is not very likely, because although neutralizing the negative charges in hERG's S1, S2, and S3 can shift the voltage dependence of activation and alter the rate of activation/deactivation, there is no effect on the kinetics or the voltage dependence (z_i) of hERG inactivation (Liu et al., 2003).

The P-helix of the hERG channel (positions 614–621 of the NH_2-terminal half of the P-loop; Fig. 1 C) (Doyle et al., 1998) can be a candidate for the inactivation voltage sensor for the following reasons. (a) An α-helix carries a dipole moment due to inducible charge separation between amide nitrogens and carbonyl oxygens of the peptide backbone. The effect can be approximated by placing 0.5–0.7 positive e_o near the NH_2 terminus and 0.5–0.7 negative e_o near the COOH terminus of such an α-helix (Hol, 1985). A calculation of the transmembrane potential profile along the axis of the KcsA channel has shown that the major portion of the transmembrane field drops across the selectivity filter (Roux et al., 2000). This is likely applicable to the hERG channel, given the well-conserved structure and function of the pore domains of all K channels. Therefore, the P-helix is within the membrane electrical field with its COOH-terminal negative dipole pointing in the inward direction. The helical dipole may sense membrane depolarization and change its position in the field. (b) The hERG channel lacks the H bond that bridges the two ends of the P-loop as in the Shaker channel (between W434/W435 and Y445, asterisks connected by a horizontal line above the Shaker sequence in Fig. 1 C) (Yang et al., 1997; Doyle et al., 1998). Therefore, the P-helix in the hERG channel may slip or rotate in response to membrane depolarization. (c) The inactivated state of the hERG channel confers a high sensitivity to drug molecules that bind to the inner cavity of the pore (Numaguchi et al., 2000). The movement of P-helices provides a logical link between conformational changes around the outer mouth (inactivation) and changes in the inner cavity (drug binding). This proposal awaits tests by direct experimental examination or by indirect theoretical calculations.

Why Are hERG and EAG So Different in their Gating Properties?

EAG channels share all the features of amino acid sequence that are proposed to be important for the unique gating properties of the hERG channel. This is exemplified by the bEAG sequence in Fig. 1. In the voltage-sensing domain, bEAG has the same extra negative charges in S1, S2, and S3, and the same positive

charges in S4 as in hERG. In the pore domain, bEAG has an even longer S5-P linker than hERG. However, EAG channels do not share the unique gating properties of the hERG channel. In low mM $[M^{2+}]_o$ (M^{2+} = Ca^{2+} and Mg^{2+}), EAG channels exhibit a much faster activation rate than hERG; at +60 mV, τ of activation <10 ms for dEAG (Silverman et al., 2000), but >50 ms for hERG. EAG channels do not manifest a fast inactivation as in hERG.

Raising $[Mg^{2+}]_o$ from 1 to 10 mM causes a pronounced slowing of EAG activation (Silverman et al., 2000; Schonherr et al., 2002). It is possible that the hERG channel operates in the $M^{2+}{}_o$-bound, slow gating mode even in normal range of $[M^{2+}]_o$ (low mM). This is suggested by the observation that lowering $[Ca^{2+}]_o$ from 1 to <0.1 mM induces a profound acceleration of hERG activation (Johnson et al., 2001), although elevating $[Ca^{2+}]_o$ from 2 to 10 mM has very modest effect (Liu et al., 2003). Therefore, the difference in the activation rate and in the sensitivity of activation rate to changes in $[M^{2+}]_o$ between hERG and EAG may be due to a difference in the set points of $M^{2+}{}_o$ binding; hERG has a high affinity $M^{2+}{}_o$ binding site (in <1 mM range) while EAG channels have a lower affinity $M^{2+}{}_o$ binding site (in 1–10 mM range).

In terms of inactivation, Fig. 1 C reveals that several positions that are critical for hERG's inactivation process are not conserved in EAG. These are highlighted by boxes on the hERG and bEAG amino acid sequences in Fig. 1 C. For example, the equivalent of hERG's S620 is T in EAG channels, and the equivalent of hERG's S631 is A in EAG channels. It has been shown that both S620T and S631A mutations in hERG greatly disrupt the inactivation process (Herzberg et al., 1998; Piper et al., 2003). Other differences between hERG and EAG may also contribute to the absence of fast inactivation in the EAG channels.

The authors would like to thank Dr. H. Robert Guy (Laboratory of Experimental and Computational Biology, National Cancer Institute, National Institutes of Health [NIH], Bethesda, MD) for constructive discussion along the course of this project.

This study was supported by RO1 HL-46451 from National Heart, Lung, and Blood Institute, NIH, and a Grant-in-Aid Award from the American Heart Association/Mid-Atlantic Affiliate (to G.-N. Tseng).

Olaf S. Andersen served as editor.

Submitted: 7 June 2004
Accepted: 13 October 2004

REFERENCES

Aggarwal, S.K., and R. MacKinnon. 1996. Contribution of the S4 segment to gating charge in the *Shaker* K^+ channel. *Neuron*. 16: 1169–1177.

Ahern, C.A., and R. Horn. 2004. Specificity of charge-carrying residues in the voltage sensor of potassium channels. *J. Gen. Physiol.* 123:205–216.

Baker, O.S., H.P. Larsson, L.M. Mannuzzu, and E.Y. Isacoff. 1998. Three transmembrane conformations and sequence-dependent displacement of the S4 domain in *Shaker* K^+ channel gating. *Neuron*. 20:1283–1294.

Bell, D.C., H. Yao, R.C. Saenger, J.H. Riley, and S.A. Siegelbaum. 2004. Changes in local S4 environment provide a voltage-sensing mechanism for mammalian hyperpolarization-activated HCN channels. *J. Gen. Physiol.* 123:5–19.

Bezanilla, F. 2000. The voltage sensor in voltage-dependent ion channels. *Physiol. Rev.* 80:555–592.

Broomand, A., R. Mannikko, H.P. Larsson, and F. Elinder. 2003. Molecular movement of the voltage sensor in a K channel. *J. Gen. Physiol.* 122:741–748.

Cohen, B.E., M. Grabe, and L.Y. Jan. 2003. Answers and questions from the KvAP structures. *Neuron*. 39:395–400.

Dascal, N. 1987. The use of *Xenopus* oocytes for the study of ion channels. *CRC Crit. Rev. Biochem.* 22:317–387.

Doyle, D.A., J.M. Cabral, R.A. Pfuetzner, A. Kuo, J.M. Gulbis, S.L. Cohen, B.T. Chait, and R. MacKinnon. 1998. The structure of the potassium channel: molecular basis of K^+ conduction and selectivity. *Science*. 280:69–77.

Emmi, A., H.J. Wenzel, P.A. Schwartzkroin, M. Taglialatela, P. Castaldo, L. Bianchi, J.M. Nerbonne, G.A. Robertson, and D. Janigro. 2000. Do glia have heart? Expression and functional role for ether-a-go-go currents in hippocampal astrocytes. *J. Neurosci.* 20:3915–3925.

Fan, J.-S., M. Jiang, W. Dun, T.V. McDonald, and G.-N. Tseng. 1999. Effects of outer mouth mutations on *hERG* channel function: a comparison with similar mutations in *Shaker*. *Biophys. J.* 76:3128–3140.

Gandhi, C.S., E. Clark, E. Loots, A. Pralle, and E.Y. Isacoff. 2003. The orientation and molecular movement of a K^+ channel voltage-sensing domain. *Neuron*. 40:515–525.

Herzberg, I.M., M.C. Trudeau, and G.A. Robertson. 1998. Transfer of rapid inactivation and sensitivity to the class III antiarrhythmic drug E-4031 from HERG to M-eag channels. *J. Physiol.* 511:3–14.

Hol, W.G. 1985. Effects of the α-helix dipole upon the functioning and structure of proteins and peptides. *Adv. Biophys.* 19:133–165.

Horn, R. 2004. How S4 segments move charge. Let me count the ways. *J. Gen. Physiol.* 123:1–4.

Hoshi, T., W.N. Zagotta, and R.W. Aldrich. 1991. Two types of inactivation on Shaker K^+ channels: effects of alterations in the carboxy-terminal region. *Neuron*. 7:547–556.

Islas, L.D., and F.J. Sigworth. 1999. Voltage sensitivity and gating charge in *Shaker* and *Shab* family potassium channels. *J. Gen. Physiol.* 114:723–742.

Jiang, Y., A. Lee, J. Chen, V. Ruta, M. Cadene, B.T. Chait, and R. MacKinnon. 2003a. X-ray structure of a voltage-dependent K^+ channel. *Nature*. 423:33–41.

Jiang, Y., V. Ruta, J. Chen, A. Lee, and R. MacKinnon. 2003b. The principle of gating charge movement in a voltage-dependent K^+ channel. *Nature*. 423:42–48.

Johnson, J.P., J.R. Balser, and P.B. Bennett. 2001. A novel extracellular calcium sensing mechanism in voltage-gated potassium ion channels. *J. Neurosci.* 21:4143–4153.

Johnson, J.P., F.M. Mullins, and P.B. Bennett. 1999. Human *ether-a-go-go*–related gene K^+ channel gating probed with extracellular Ca^{2+}. Evidence for two distinct voltage sensors. *J. Gen. Physiol.* 113:565–580.

Kiehn, J., A.E. Lacerda, B. Wible, and A.M. Brown. 1996. Molecular physiology and pharmacology of HERG. Single-channel currents and block by dofetilide. *Circulation*. 94:2572–2579.

Laine, M., M.-C.A. Lin, J.P.A. Bannister, W.R. Silverman, A.F. Mock, B. Roux, and D.M. Papazian. 2003. Atomic proximity between S4 segment and pore domain in Shaker potassium channels. *Neu-*

ron. 39:467–481.

Larsson, H.P., and F. Elinder. 2000. A conserved glutamate is important for slow inactivation in K^+ channels. *Neuron.* 27:573–583.

Larsson, H.P., O.S. Baker, D.S. Dhillon, and E.Y. Isacoff. 1996. Transmembrane movement of the shaker K^+ channel S4. *Neuron.* 16:387–397.

Lee, H.C., J.M. Wang, and K.J. Swartz. 2003. Interaction between extracellular hanatoxin and the resting conformation of the voltage-sensor paddle in Kv channels. *Neuron.* 40:527–536.

Liu, J., M. Zhang, M. Jiang, and G.-N. Tseng. 2002. Structural and functional role of the extracellular S5-P linker in the HERG potassium channel. *J. Gen. Physiol.* 120:723–737.

Liu, J., M. Zhang, M. Jiang, and G.-N. Tseng. 2003. Negative charges in the transmembrane domains of the HERG K channel are involved in the activation and deactivation gating processes. *J. Gen. Physiol.* 121:599–614.

Logothetis, D.E., S. Movahedi, C. Satler, K. Lindpaintner, and B. Nadal-Ginard. 1992. Incremental reductions of positive charge within the S4 region of a voltage-gated K^+ channel result in corresponding decreases in gating charge. *Neuron.* 8:531–540.

Numaguchi, H., F.M. Mullins, J.P.J. Johnson, D.C. Johns, S.S. Po, I.C.H. Yang, G.F. Tomaselli, and J.R. Balser. 2000. Probing the interaction between inactivation gating and d-sotalol block of *HERG. Circ. Res.* 87:1012–1018.

Papazian, D.M., W.R. Silverman, M.-C.A. Lin, S.K. Tiwari-Woodruff, and C.-Y. Tang. 2002. Structural organization of the voltage sensor in voltage-dependent potassium channels. *Novartis Foundation Symposium.* 245:178-192.

Piper, D.R., A. Varghese, M.C. Sanguinetti, and M. Tristani-Firouzi. 2003. Gating currents associated with intramembrane charge displacement in HERG potassium channels. *Proc. Natl. Acad. Sci. USA.* 100:10534–10539.

Rosati, B., P. Marchetti, O. Crociani, M. Lecchi, R. Lupi, A. Arcangeli, M. Olivotto, and E. Wanke. 2000. Glucose- and arginine-induced insulin secretion by human pancreatic β-cells: the role of HERG K^+ channels in firing and release. *FASEB J.* 14:2601–2610.

Roux, B., S. Berneche, and W. Im. 2000. Ion channels, permeation, and electrostatics: insight into the function of KcsA. *Biochemistry.* 39:13295–13306.

Sanguinetti, M.C., C. Jiang, M.E. Curran, and M.T. Keating. 1995. A mechanistic link between an inherited and an acquired cardiac arrhythmia: HERG encodes the I_{Kr} potassium channel. *Cell.* 81: 299–307.

Schonherr, R., L.M. Mannuzzu, E.Y. Isacoff, and S.H. Heinemann. 2002. Conformational switch between slow and fast gating modes: allosteric regulation of voltage sensor mobility in the EAG K^+ channel. *Neuron.* 35:935–949.

Schoppa, N.E., K. McCormack, M.A. Tanouye, and F.J. Sigworth. 1992. The size of gating charge in wild-type and mutant Shaker potassium channels. *Science.* 255:1712–1715.

Schreibmayer, W., H.A. Lester, and N. Dascal. 1994. Voltage clamping of *Xenopus laevis* oocytes utilizing agarose-cushion electrodes. *Pflugers Arch.* 426:453–458.

Seoh, S.-A., D. Sigg, D.M. Papazian, and F. Bezanilla. 1996. Voltage-sensing residues in the S2 and S4 segments of the *Shaker* K^+ channel. *Neuron.* 16:1159–1167.

Shoeb, F., A.P. Malykhina, and H.I. Akbarali. 2003. Cloning and functional characterization of the smooth muscle ether-a-go-go-related gene K^+ channel. *J. Biol. Chem.* 278:2503–2514.

Silverman, W.R., B. Roux, and D.M. Papazian. 2003. Structural basis of two-stage voltage-dependent activation in K^+ channels. *Proc. Natl. Acad. Sci. USA.* 100:2935–2940.

Silverman, W.R., C.-Y. Tang, A.F. Mock, K.-B. Huh, and D.M. Papazian. 2000. Mg^{2+} modulates voltage-dependent activation in Ether-a-go-go potassium channels by binding between transmembrane segments S2 and S3. *J. Gen. Physiol.* 116:663–677.

Smith, P.L., T. Baukrowitz, and G. Yellen. 1996. The inward rectification mechanism of the HERG cardiac potassium channel. *Nature.* 379:833–836.

Smith, P.L., and G. Yellen. 2002. Fast and slow voltage sensor movements in HERG potassium channels. *J. Gen. Physiol.* 119:275–293.

Starace, D.M., and F. Bezanilla. 2004. A proton pore in a potassium channel voltage sensor reveals a focused electric field. *Nature.* 427:548–553.

Tiwari-Woodruff, S.K., M.-C.A. Lin, C.T. Schulteis, and D.M. Papazian. 2000. Voltage-dependent structural interactions in the *Shaker* K^+ channel. *J. Gen. Physiol.* 115:123–138.

Torres, A.M., P. Bansal, M. Sunde, C.E. Clarke, J.A. Bursill, D.J. Smith, A. Bauskin, S.N. Breit, T.J. Campbell, P.F. Alewood, et al. 2003. Structure of the HERG K^+ channel S5P extracellular linker: role of an amphipathic α-helix in C-type inactivation. *J. Biol. Chem.* 278:42136–42148.

Tristani-Firouzi, M. 2004. Voltage sensor movement in hERG channels as measured by gating currents. *Novartis Foundation Symposium.* In press.

Tseng-Crank, J.C.L., G.-N. Tseng, A. Schwartz, and M.A. Tanouye. 1990. Molecular cloning and functional expression of a potassium channel cDNA isolated from a rat cardiac library. *FEBS Lett.* 268:63–68.

Wang, M.H., S.P. Yusaf, D.J.S. Elliott, D. Wray, and A. Sivaprasadarao. 1999. Effects of cysteine substitutions on the topology of the S4 segment of the Shaker potassium channel: implications for molecular models of gating. *J. Physiol.* 521:315–326.

Yang, Y., Y.-Y. Yang, and F.J. Sigworth. 1997. How does the W434F mutation block current in *Shaker* potassium channels? *J. Gen. Physiol.* 109:779–789.

Zagotta, W.N., and R.W. Aldrich. 1990. Voltage-dependent gating of shaker A-type potassium channels in *Drosophila* muscle. *J. Gen. Physiol.* 95:29–60.

Zagotta, W.N., T. Hoshi, J. Dittman, and R.W. Aldrich. 1994. Shaker potassium channel gating II: transitions in the activation pathway. *J. Gen. Physiol.* 103:279–319.

Zhou, W., F.S. Cayabyab, P.S. Pennefather, L.C. Schlichter, and T.E. DeCoursey. 1998. HERG-like K^+ channels in microglia. *J. Gen. Physiol.* 111:781–794.